AIAA AVIATION Forum
August 2-6, 2021, VIRTUAL EVENT
AIAA AVIATION 2021 FORUM

10.2514/6.2021-2696

Prototype Development of a Variable Altitude Venus Aerobot

Jeffery L. Hall,[1] Michael T. Pauken,[2] Aaron Schutte,[3] Siddharth Krishnamoorthy,[4] Carolina Aiazzi[5] and Jacob S. Izraelevitz[6]
Jet Propulsion Laboratory, California Institute of Technology, Pasadena, CA., 91109, USA.

Tim Lachenmeier[7] and Caleb Turner[8]
Near Space Corporation, Tillamook, OR, 97141, USA.

This paper presents the design methodology and results from the first subscale prototype of a variable altitude Venus aerobot jointly developed by JPL and Near Space Corporation. This vehicle is based on the principle of a two-part balloon for which pumping helium gas between the balloons can modulate buoyancy and thereby control the altitude of the vehicle. The intended mission application at Venus is a cloud-level exploration across an altitude range of 52 to 62 kilometers for weeks or months, circumnavigating the planet multiple times and carrying an approximately 100 kg payload module containing all scientific instruments, avionics and other vehicle support systems. The first prototype is approximately one-third scale (4 m diameter) and serves as a proof-of-concept test article allowing for evaluation of manufacturing approaches and laboratory testing to evaluate performance. Two key design features of the prototype as built are the use of Teflon film on the outside of the balloon to protect it from the sulfuric acid aerosols in the Venusian atmosphere and second surface metallization of that film to reflect most incident sunlight and thereby limit diurnal temperature and the associated temperature-driven pressure fluctuations. This prototyping effort has been complemented with a detailed vehicle simulation activity that incorporates the relevant balloon physics and thereby models the expected dynamic behavior of the aerobot in both the Earth and Venus atmospheres. Data obtained in laboratory tests of the prototype have been used to validate, verify and update that simulation model as described in the paper.

I. Nomenclature

A	=	area of balloon, as function of arclength
b	=	internal pressure slope
C_d	=	discharge coefficient of the pump
C_D	=	balloon drag coefficient
c_g	=	helium specific heat
C_m	=	virtual mass coefficient
d	=	vent orifice diameter
F_b	=	buoyancy force generated by the gas
g	=	gravitational constant (Earth or Venus)
$\dot{H}_1$	=	enthalpy rate with respective to time for the gas being vented in the ZP balloon
$\dot{H}_2$	=	enthalpy rate with respective to time for the gas being pumped out of the ZP balloon
m	=	component mass
M_{total}	=	total floating mass
P	=	pressure
Q	=	heat flux (radiative or convective)
$\dot{q}$	=	net thermal heat transfer
r	=	radius
r_g	=	radius along the gore
R_{He}	=	ideal gas constant of helium

s = arc length along the gore
S_{ref} = external cross-sectional area of the zero-pressure balloon
T = temperature
t = time
V = balloon's volume
$\dot{V}_{pump}$ = pump volume rate expressed in liters per minute
v_{wind} = vertical wind speed
w = areal density of the balloon's material
z = altitude
z_0 = hydrostatic point on the balloon
Atm = subscript denoting atmosphere
He = subscript denoting helium
SP = subscript denoting superpressure balloon
ZP = subscript denoting zero-pressure balloon
α = solar absorptivity
α_c = cone angle for ZP balloon shape function
β = angle from the center-line to the point where the external envelope is detaching from the SP balloon, clockwise
ϵ = infrared emissivity
ρ = gas density
θ = vertical tangent angle to the balloon
σ = Stefan–Boltzmann constant
σ_c ,σ_m = circumferential and meridional stresses

II. Introduction

There have been many studies and technology development efforts to create a new balloon-based vehicle for Venus ever since the two original VeGa balloon flights at that planet in 1985 [1-7]. A key driver has been the desire for long duration flights in the Venusian atmosphere to maximize science return. The use of buoyancy to provide the vehicle lift without power consumption is particularly valuable at Venus given the fact that such a vehicle must spend long periods (50-70 hours) in darkness as it flies around the planet, a time for which battery-stored energy is scarce.

In recent years the concept of a variable altitude balloon has emerged as a preferred candidate. In this option, the balloon vehicle has a buoyancy modulation capability that allows it to traverse a roughly 10 km altitude range in a repeatable fashion without dropping ballast or venting helium buoyancy gas. This significantly enhances the scientific utility of the platform by covering a large range of altitudes. Such a controlled robotic balloon-based vehicle is typically referred to as an "aerobot". The variable altitude aerobot concept was specifically recommended in the 2018 NASA-sponsored study on Venus Aerial platforms that assessed a wide assortment of aerial vehicle types that also included a fixed altitude balloon and a solar-powered aircraft [8]. This recommendation in part stemmed from the fact that current and recent terrestrial balloons already had demonstrated the principle of altitude control via gas pumping such as the Google Loon [9], World View Stratolite [10], Near Space WindStar, and the Controlled Meteorological (CMET) balloon [11]. With the basic premise of operation already established by these terrestrial balloon examples, the challenge becomes a modest adaptation of the technology for the Venus environment.

There are a number of options for implementing a variable altitude aerobot for Venus and these were investigated in a subsequent research activity that developed the fundamental thermodynamic theory and performed a mass and power trade study amongst the leading candidates [12]. It found that the most mass and energy efficient option for a Venus variable altitude aerobot is a pumped helium, balloon-in-a-balloon design (Fig. 1). The inside balloon in this concept is always pressurized (making it a de facto superpressure or SP balloon) while the outside balloon is unpressurized (making it a zero pressure or ZP balloon) that expands or contracts depending on the helium gas distribution and altitude. Moving helium gas between the two balloons modulates the buoyancy and effects altitude changes. Note the operational asymmetry in that a pump is required to move gas from the outside to the inside balloon while simple venting through an orifice allows the reverse flow.

This balloon-in-a-balloon design features two other key advantages at Venus:

- Any helium gas that leaks out of the inner SP balloon is captured by the outer ZP balloon and not lost. The net effect will be a small increase in pumping energy required to put it back into the SP balloon.
- The inner balloon is protected by the outer balloon from the sulfuric acid aerosols in the Venusian clouds allowing for the inner balloon structure to be optimized for strength to carry the pressure loads. This leads to a more reliable, mass efficient structure.

Further technical details concerning this concept are presented in the next section.

This balloon-in-a-balloon version of the Venus variable altitude aerobot was baselined in the NASA 2020 Venus Flagship Mission (VFM) study [13]. That vehicle was quite large for which a 15 m diameter ZP balloon and 7.5 m diameter SP balloon were required to carry the 216 kg gondola mass containing all science instruments and supporting subsystems. However, it should be noted that this aerobot technology is scalable and that much smaller and larger options are possible as needed to satisfy the mission objectives. The VFM aerobot was intended to operate for 60 Earth days and fly between a 52 km and 62 km altitude range at Venus. For comparison purposes, a Venus aerobot operating across the same altitude range but with only a 100 kg gondola will result in an 11.5 m diameter ZP balloon.

The next sections of this paper present results in three key areas:

- A description of the current design approach for the Venus aerobot including the margining strategy that should yield a robust design given the realities of material and manufacturing inefficiencies and the environmental effects of solar heating and vertical winds.
- Details on the first sub-scale prototype balloon built and tested in a laboratory environment as a proof of concept.
- A description of the JPL simulation tool developed to model aerobot flight on Earth and on Venus. This includes some sample calculations and comparisons to the laboratory test results of the prototype balloon.

III.Balloon Design Approach

A. Model Description

As initially discussed in Hall et al. [12], we employ steady-state equilibrium models for the design of these aerobots, which are then validated against dynamic simulations and subscale prototypes. This equilibrium model, while simplified, captures enough of the relevant physics to allow parametric studies of multiple design points, and is flexible enough to allow tailoring to lessons learned. For more details on the model, we refer the reader to Hall et al. [12], of which a few relevant equations are reproduced here.

Central to this model is the buoyancy relation:

$$\rho_{atm}V_{zp} + \rho_{atm}V_{sp} = M_{total} - \hat{v}_{wind}\frac{1}{2}\rho_{atm}S_{ref}(v_{wind})^2 C_D/g \tag{1}$$

where $\rho_{atm}V_{zp}$ and $\rho_{atm}V_{sp}$ are the buoyancy (in kilograms) provided by the zero-pressure and superpressure balloons respectively in the Venus atmosphere (Fig. 1), M_{total} is the total floating mass, and $\hat{v}_{wind}\frac{1}{2}\rho S_{ref}(v_{wind})^2 C_D/g$ is the vertical wind drag converted to kilograms. The frontal (cross-sectional) area of the balloon S_{ref} is a function of the volume of each balloon (and therefore temperature), for which we assume ideal gas behavior:

$$V_{zp} = m_{He,zp}R_{He}T_{zp}/P_{atm} \tag{2}$$

$$V_{sp} = m_{He,sp}R_{He}T_{sp}/P_{sp} \tag{3}$$

where the zero-pressure balloon internal pressure P_{zp} is known to be the same as the external atmosphere, and P_{sp} is the pressure in the SP balloon that is by definition always above the local atmospheric pressure. Determining the balloon temperature requires an equilibrium thermal solution that balances the solar and IR fluxes (and their view factors) with the convection off the surface of the balloon.

$$0 = \frac{1}{2}\alpha Q_{solar,down} + \frac{1}{2}\alpha Q_{solar,up} + \frac{1}{4}\alpha Q_{solar,direct} + \frac{1}{2}\epsilon Q_{IR,down} + \frac{1}{2}\epsilon Q_{IR,up} - Q_{convection} - \sigma\epsilon {T_{zp}}^4 \tag{4}$$

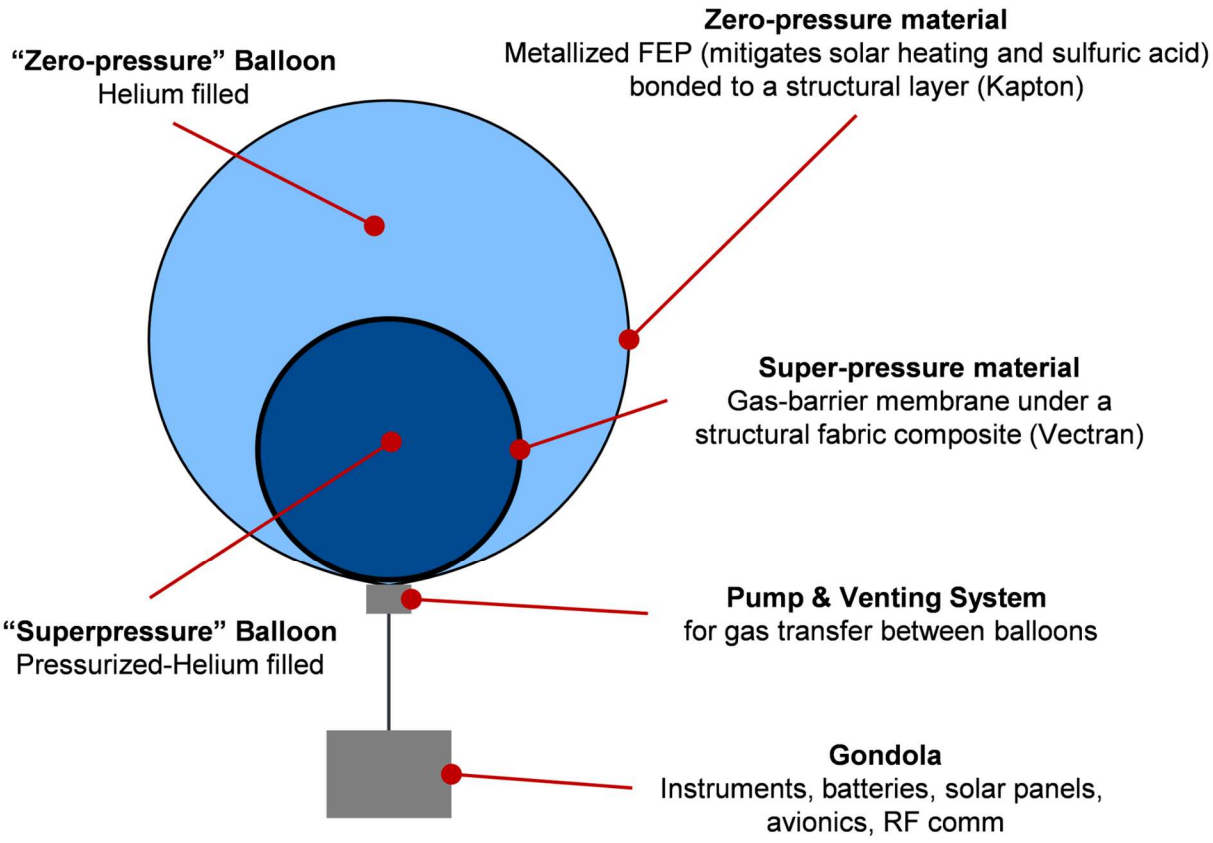

Fig. 1 Balloon-in-balloon Variable-Altitude Aerobot Architecture.

where α is the solar absorptivity, ϵ is the IR emissivity, Q_{solar} is the down and up solar power flux, Q_{IR} is the down and up infrared power flux, $Q_{convection}$ is the power flux to the balloon due to convective heat transfer with the atmospheric gas, T_{zp} is the temperature of the zero pressure balloon envelope and σ is the Stefan Boltzmann constant.

For any given altitude, the thermal model must be first solved to determine the balloon temperature, followed by iterating on the helium mass distribution between both balloons to meet the buoyancy constraint for a given vertical wind. The total mass of the aerobot includes the balloons (envelopes), the helium gas and the carry mass in the gondola:

$$M_{total} = m_{He,zp}+m_{He,sp} + m_{zp,envelope} + m_{sp,envelope} + M_{gondola} \quad (5)$$

Where $m_{He,zp}+m_{He,sp}$ is the fixed total mass of helium distributed between balloons, $m_{zp,envelope}$ and $m_{sp,envelope}$ are the masses of each balloon envelope and associated end fittings, and $M_{gondola}$ is the hanging mass below the balloons.

B. Design Points

Different investigated design points represent different assumed models for the mass of each balloon envelope, thermal model coefficients, targeted wind drag, and other such assumptions, uncovered through an improving understanding of the Venus environment and lab feasibility experiments of assembling Venus-relevant balloons. A comparison of key investigated design points is tabulated in Table 1, with additional information in the following section. The final column in Table 1 illustrates the as-built performance of the current subscale prototype used in the testing and simulations described below.

1. Original Design Point "A"

The original design points of Hall et al. [12] assumed:

- An altitude range from 52-60 km or 52-62 km for nominal operations of the balloon, with expected excursions beyond this range due to perturbing vertical winds.
- A worst-case sustained vertical wind gust of magnitude 3 m/s, as informed by the 1985 VeGa balloon flights
- A small pressurization margin in the SP balloon of 1000 Pa beyond the pressure seen during the worst-case sustained downdraft, allowing the balloon to maintain its fully inflated shape that, as for all superpressure balloons, also provides for passive altitude stability at all points in the mission.
- Venus International Reference Atmosphere (VIRA) model for the environmental properties of the Venus atmosphere [14].
- A 100 kg suspended gondola - including the science instruments, flight avionics, solar panels, batteries, communications, and pumping system for transferring gas between balloons.
- The mass of the ZP and SP balloon envelopes was estimated by adding a 30% construction factor on top of the basic mass per unit area of the parent material that approximately accounts for the additional mass of gore-to-gore seams, polar end cap feedthroughs for gas transfer, and all other localized structural reinforcements. A further mass margin of 20% was then added to account for future mass growth as the technology development process proceeds.
- A drag coefficient of 0.5 for any balloon-relative wind on the inflated balloon (separated flow) with an assumed spherical shape.

These design points represented the first closed aerobot designs for a balloon-in-balloon architecture for Venus, with a float mass including helium of 210.1 kg (for an altitude range of 52-60 km) and 229.6 kg (for 52-62 km). The higher altitude understandably requires a slightly larger balloon to generate sufficient buoyancy in the less dense higher atmosphere.

2. Updated Design Points "B"

Technology development since 2019 indicated the need for several modifications to these design inputs.

1. Variation in balloon volume ratio: The original design points in Hall et al. [12] assumed a 1:2 diameter ratio between the internal SP balloon and the external ZP balloon. This ratio is not necessarily optimal, and so a trade study was conducted to evaluate this degree-of-freedom. Design points B0, B1 and B2 in Table 1 summarize the results of this trade. In general, maximizing the size of the SP balloon (point B2) saves mass and pressure loading, though it incurs a minor energy increase by running a higher throughput pump.
2. Improved predictions for the Venus Solar/IR Flux Environment: Rather than the simplistic linear model employed in Hall et al. [12], a more realistic radiative flux model was obtained from Robinson et al. 2018 [15], allowing for specific solar absorptivity and infrared emissivity to be evaluated as a function of altitude. The effect of solar and infrared heating, and its associated increased pressures, are now better understood and factored into the designs.
3. Realistic ZP balloon material: Initial prototyping with thermal control materials settled on a metallized bilayer of Teflon & Kapton (see section IV.A), which provides a good combination of sulfuric acid resistance, helium retention and minimized solar heating. This new ZP baseline material is slightly lighter than the assumed material from the original paper [12].
4. Robust margining for SP balloon fabric mass: Lessons learned from prior Venus superpressure balloon developments (including References [6] and [7]) have been incorporated into a new margining approach for the SP balloon design. This generally adds further tensile strength reduction (knockdown) factors as compared to the ideal tensile strength of the fabric material as measured by uniaxial load tests. We find it helpful to think about this as a three-step process, specifically:

$$[\text{Uniaxial Failure}] = [\textit{Crimp knockdown}] * [\textit{Num. Fibers}] * [\text{Minimum Fiber Strength}] \quad (6)$$

$$[\text{Biaxial Failure}] = [\textit{Seam knockdown}] * [\textit{Biaxial knockdown}] * [\text{Uniaxial Failure}] \quad (7)$$

$$[\text{Operational Strength}] = [1/\text{FOS}] * [\textit{Thermal Knockdown}] * [\text{Biaxial Failure}] \quad (8)$$

Table 1: Venus Aerobot Design Points

	Hall et al. 2019	Hall et al. 2019	Design B0	Design B1	Design B2	Subscale Prototype
Operating Parameters						
Operating Altitude Range (km)	52-60	52-62	52-62	52-62	52-62	-----
ZP Envelope Diameter (m)	10.6	11.6	13.5	13	12.5	3.9
SP Envelope Diameter (m)	5.3	5.8	6.5	6.7	7.0	2.0
ZP Envelope Areal Density (g/m2)	120	120	95	95	95	95
SP Envelope Areal Density (g/m2)	170	170	250	225	200	250
Alpha & Epsilon	---	---	0.09, 0.48	0.09, 0.48	0.09, 0.48	0.08, 0.52
Minimum Superpressure (Pa)	1,000	1,000	1,000	1,000	1,000	500
Maximum Superpressure (Pa)	32,800	28,100	31,500	27,300	22,700	7,000
Energy (at 70% efficiency) to descend in Daytime (WHr)	500	740	1150	1160	1180	---
Maximum Perturbed Altitude (km)	62	63.6	64.5	64.0	63.5	---
Mass Breakdown						
ZP Envelope Mass (kg)	66.1	79.2	84.9	78.7	72.7	6.8
SP Envelope Mass (kg)	23.4	28.0	51.8	49.5	48.1	9.2
Helium Mass (kg)	20.6	22.4	25.6	24.7	23.7	3.8
Gondola Mass (kg)	100	100	100	100	100	9.0
Total Floating Mass (kg)	**210.1**	**229.6**	**262.2**	**252.9**	**244.5**	**28.8**

where standard Vectran fibers are generally specified at a minimum of 23 gram-force per denier. Knockdown strengths can vary significantly based on weave parameters, but a conservative rule-of-thumb before load testing is to adopt a crimp knockdown of 20%, biaxial knockdown of 23%, seam knockdown of 20%, and a linear thermal knockdown of 0% at 20°C to 25% at 100 °C. Operational pressures assume a factor-of-safety of 2X beyond these knockdowns. The SP balloon material masses in Table 1 include this complete knockdown architecture for the Vectran fabric mass predictions, plus an additional 45 g/m2 allowance for the polyurethane film gas barrier.

5. Temperature under vertical winds: Initial dynamic simulations of aerobots in vertical winds indicated a significant thermal lag, where the balloon temperature would vary slower than the outside atmosphere. This has the effect of exacerbating altitude changes - as a balloon displaced upwards will initially be too hot (and more buoyant) than equilibrium predictions and similarly a balloon displaced downwards will be too cold. To first order, this can be conservatively handled by assuming an isothermal (instead of equilibrium) balloon gas during wind drafts. The new set of balloon designs in Table 1 include this new assumption, and accordingly recommend larger SP balloons to provide extra altitude stability to offset the effect.

Figure 2 illustrates the predicted performance of Design Case B2, which has the largest superpressure balloon of the family and strongest altitude stability. For each altitude extrema in day and night, the shaded polygon shows excursion due to updrafts/downdrafts at 3 m/s. Similar to other balloons of the same family, the highest pressures are seen during local noon, when the solar heating is at its peak, while at night, conditions are much more benign. Comparing the helium equilibrium helium mass in day and night offers a window into the pump's operation. In

daylight much more helium is needed to be stored in the SP balloon in order to compensate for the increased buoyancy of the hotter gas in the ZP balloon. Positive superpressure is maintained at all times (Figure 2a).

IV.Subscale Prototype Description

In this section we describe the first subscale prototype of a Venus balloon-in-a-balloon aerobot designed and fabricated by JPL and Near Space Corporation. The purpose was to evaluate manufacturing approaches and to produce a moderate fidelity prototype that could be tested in the laboratory and compared to the design assumptions described above. These experimental data were also used to start the validation process of a physics-based aerobot simulation model at JPL that is described in Section VI.

A. Balloon Description

Some compromises were made in the design of the first prototype balloons in an effort to balance cost, development time and performance. These mostly pertained to the SP balloon that was constructed from Spectra fabric. Spectra is sufficient for Earth testing but does not have the required high temperature (up to 100 °C) performance required for operation at 52 km on Venus. In contrast, the zero pressure balloon material was developed to closely match the performance required for use at Venus and in particular incorporated these key design features:

- Resist the corrosive effects of the sulfuric acid aerosols in the Venus clouds
- Carry the mass loads of the payload
- Minimize solar heating
- Minimize helium gas loss

No single polymer film material is known to fully meet the requirements in each of these areas. Therefore, a bi-laminate film was developed to meet all the requirements. The design of the bi-laminate film is illustrated in Figure 3. The outer layer of the zero-pressure balloon envelope is a 1-mil (25 micron) thick fluorinated ethylene propylene (FEP) film to provide corrosion resistance. The FEP is metalized on the back surface with silver then Inconel (to provide oxidation resistance). The FEP film layer is bonded with a thermoset adhesive to a 1-mil thick polyimide film. The area mass density of the bi-laminate film is 95 g/m^2. The polyimide film provides the strength to support the payload mass load on the balloon during all balloon mission phases. The silver metallization provides both a helium gas barrier (permeability < 5 cc/m^2-day as measured at room temperature) and a second surface optical mirror to minimize solar heating loads on the balloon. Both the FEP and the thermoset adhesive are transparent to take advantage of the low solar absorptivity ($\alpha < 0.09$ measured) of the silver layer. The FEP is a dielectric material and provides a high emissivity ($\varepsilon > 0.5$ measured) to promote heat loss from the balloon via thermal radiation in addition to convective heat loss to the atmosphere. The zero-pressure balloon gores are attached to each other using a polyimide tape with pressure sensitive adhesive (PSA) on the interior surface. Corrosion protection on the outside gore seams is provided by a cover tape of FEP bonded to the gores with a silicone PSA.

The super-pressure balloon material was designed to meet strength requirements to contain the pressure load of the helium storage reservoir. As mentioned above, the current design features a Spectra fabric layer with an area mass density of the fabric was 203 g/m^2. The super-pressure balloon gores secured to each other with sewn seams. A 1.5-mil thick polyurethane film gas barrier bladder was placed inside the Spectra shell. The gores of the polyurethane film bladder were secured together with a radio-frequency (RF) welder. The gas permeability of the super pressure balloon is not as stringent as the zero-pressure balloon because a small gas leakage can be overcome by the balloon helium pump. Therefore, metallization of the polyurethane film is not needed. Future plans for the super pressure balloon design will laminate the polyurethane film to a Vectran fabric instead of using Spectra fabric with a gas bladder approach. While the internal Spectra superpressure balloon material was selected to reach superpressures relevant for Venus, the initial testing was done at relatively low superpressure below 7000 Pa (1 psi).

The zero-balloon was fabricated in the shape of a 3.9 m diameter sphere-cone, tapered at 60 degrees, with the 2 m-diameter superpressure balloon lying at its bottom apex. The conical shape allows nesting between the two balloons and provides a means of efficiently spreading the gondola payload weight and carrying it to the top gas bubble. Compared to the Design Point B2, this represents an approximately 3:1 subscale model, and allows for verification of the outer material manufacturability, the balloon-in-balloon architecture, the suspension load path to both chambers, and the pumping & venting scheme for adjusting altitude.

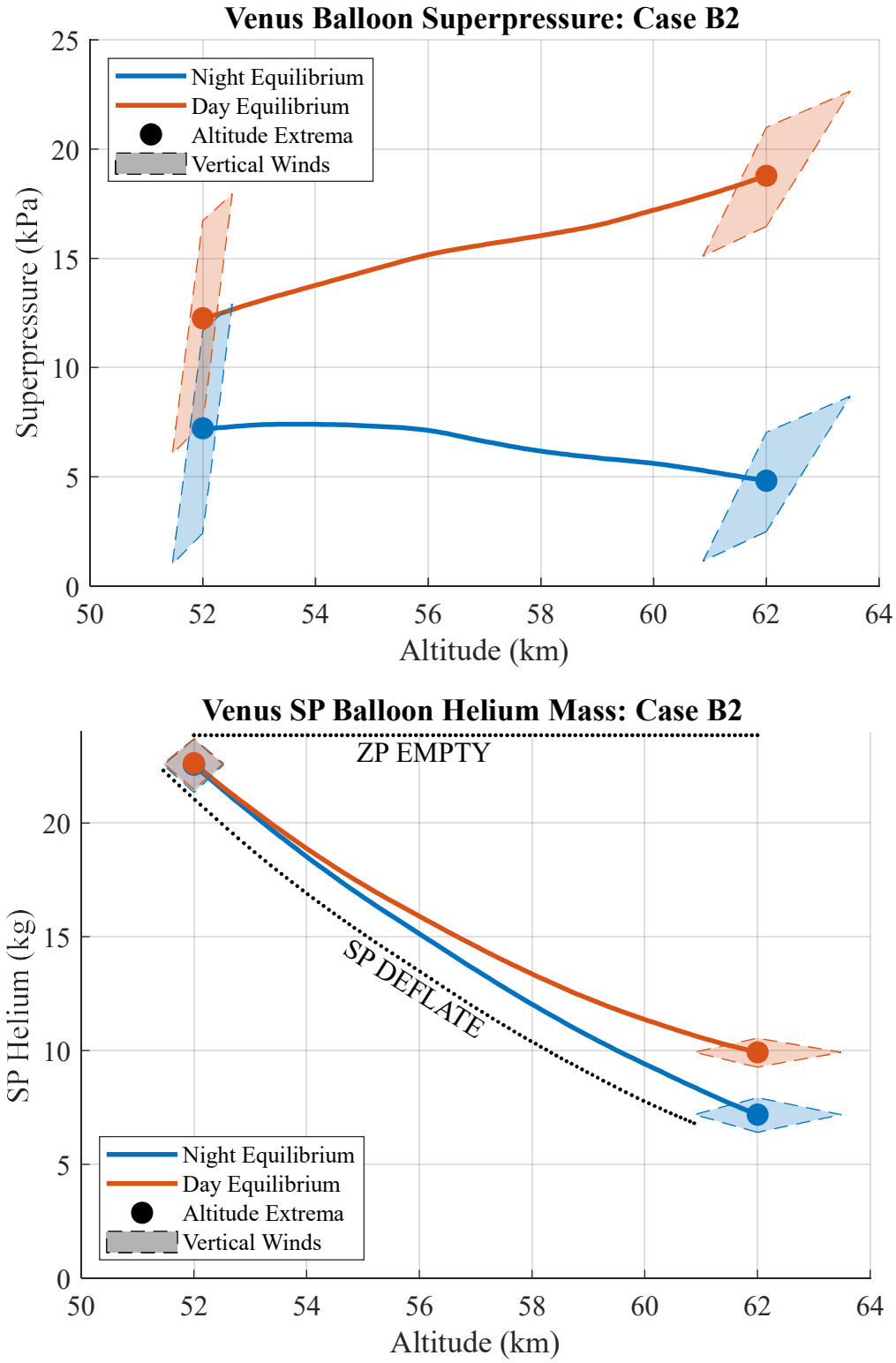

Fig. 2 Performance of Aerobot Design B2 as predicted by design model. Top (a): Equilibrium superpressure as a function of altitude. Bottom (b): Helium mass inside SP balloon, including boundaries of when the ZP balloon becomes empty or the SP balloon becomes deflated.

Fig. 3 Illustration of zero-pressure balloon bi-laminate film material lay-up.

B. Experiment Electronics and Sensors

The electronics system was designed to actuate the pumping system for the aerobot and collect engineering data relating to its performance. Our first test of the subscale prototype employed rapid-prototyping and commercial-off-the-shelf (COTS) solutions to rapidly conduct the first test and gather essential data. The electronics system may be broadly divided into two parts:

1. Pumping electronics
2. Engineering data acquisition

B.1. Pumping Electronics

The pumping system for the aerobot consists of two solenoid valves and a pump to move helium between the outer ZP balloon and the inner SP balloon. Each of the three components of the pumping electronics system was actuated using a DC-relay board and a 24-V battery as shown in Figure 4.

B.2. Engineering data acquisition

Laboratory (indoor) testing of the aerobot prototype requires significant engineering data to quantify vehicle performance and enable comparisons to the pre-test predictions from the FLOATS simulation model. We therefore incorporated sensors onto the vehicle to collect the following data during our tests:

1. Atmospheric pressure and temperature
2. ZP balloon gas pressure and temperature
3. SP balloon gas pressure and temperature
4. Skin temperature at the north pole, south pole and middle of the aerobot
5. Vehicle (gondola) height
6. Pump and valve states

A schematic diagram for the data acquisition system in Figure 5. All instruments were synchronized using the CPU clock of the Raspberry Pi and synchronized with wall-clock time using the GPS time base provided by the IMU.

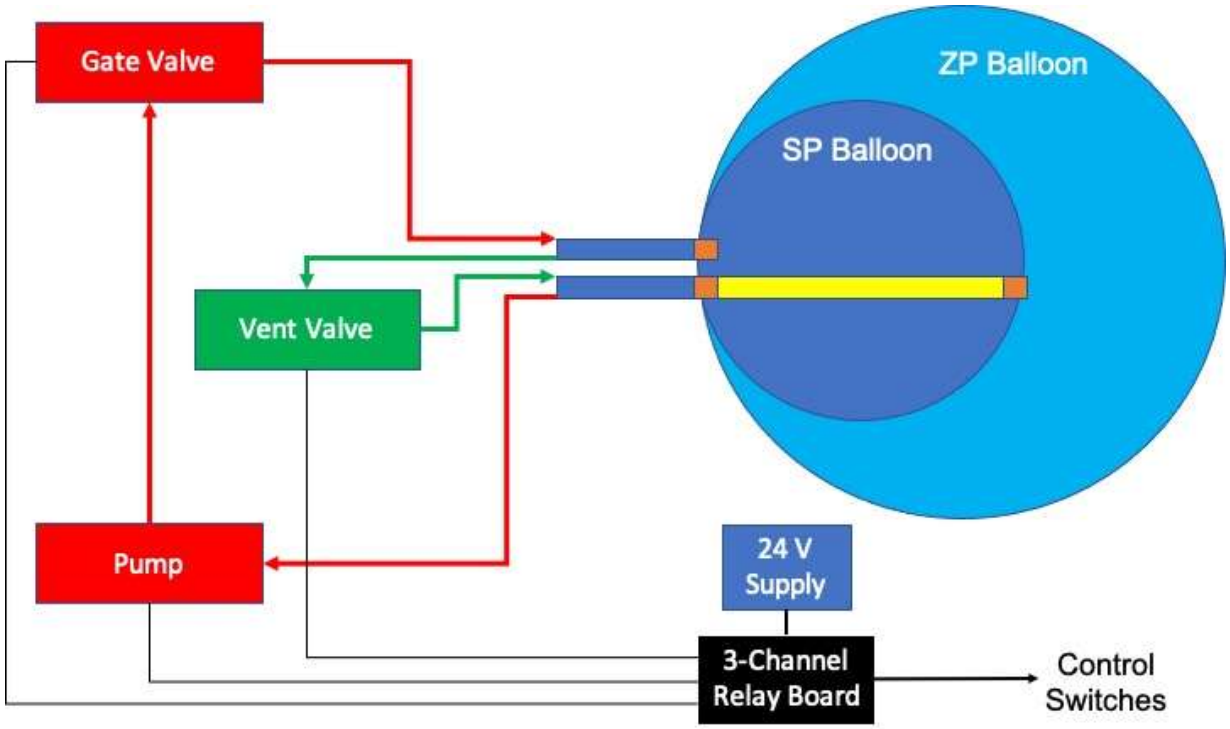

Figure 4: The pumping system for the aerobot. The red and green arrows indicate the gas path. Black lines show electronic lines. The three elements are powered by 24 V batteries and DC relays.

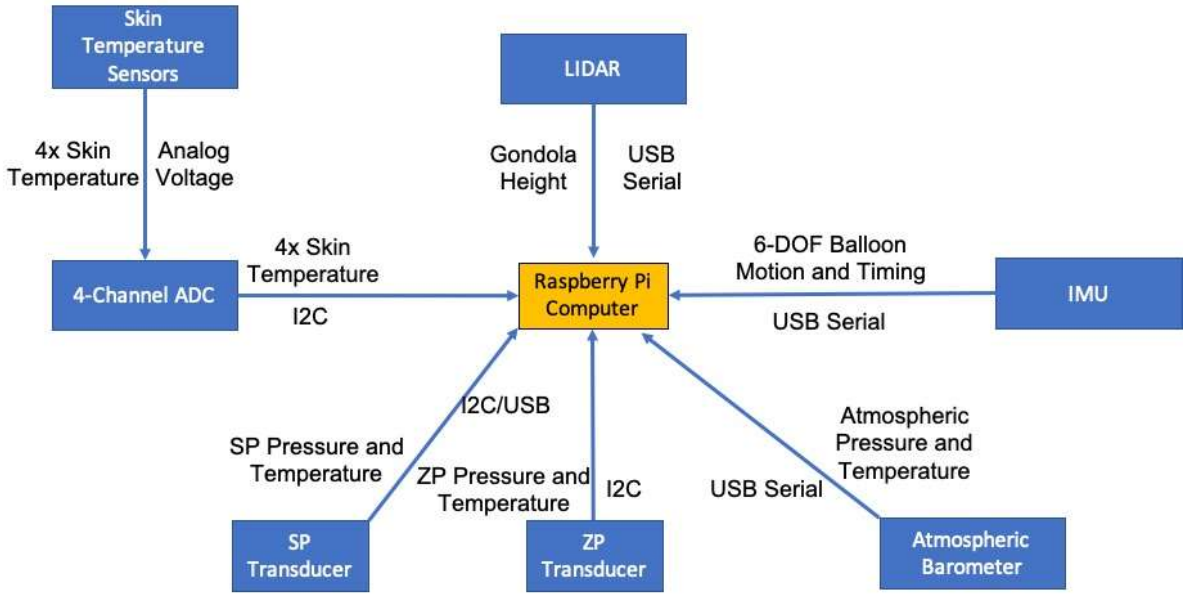

Figure 5: Schematic for electronics for the aerobot subscale test. Instruments communicated the atmospheric state, and aerobot thermal and dynamic state with a Raspberry Pi single-board computer using I2C and USB-Serial communication protocols. Pump and valve states were monitored manually.

C. Integrated aerobot

The assembled subscale aerobot (including both the gondola payload and the two balloon envelopes) is shown in Figure 6. The bottom structural end fitting provides gas access to both balloons via two ports: one port directly enters the SP balloon and the other port accesses the ZP balloon through an internal hose. A small transparent window (made of Mylar) provides visual access to the SP balloon during the test and would not be included in a full-scale balloon. The subscale balloon itself is ~5.5 meters tall and the gondola hangs an extra meter below. For the test, the balloon was manually commanded to ascend and descend under its own battery power, and performance logged using the gondola electronics and instrumentation. Four tethers and two gas lines connect the gondola to the end fitting.

The peanut-like underinflated balloon shape in Figure 6, where the gas in the ZP balloon rises above the SP balloon, would be typical for most of the balloon mission on Venus. The ZP balloon only gets fully inflated during the worst-case updraft at high altitude, so the volume deficit creates excess material around the balloon midsection. This midsection expands and contracts with altitude as gas is exchanged between the balloon chambers.

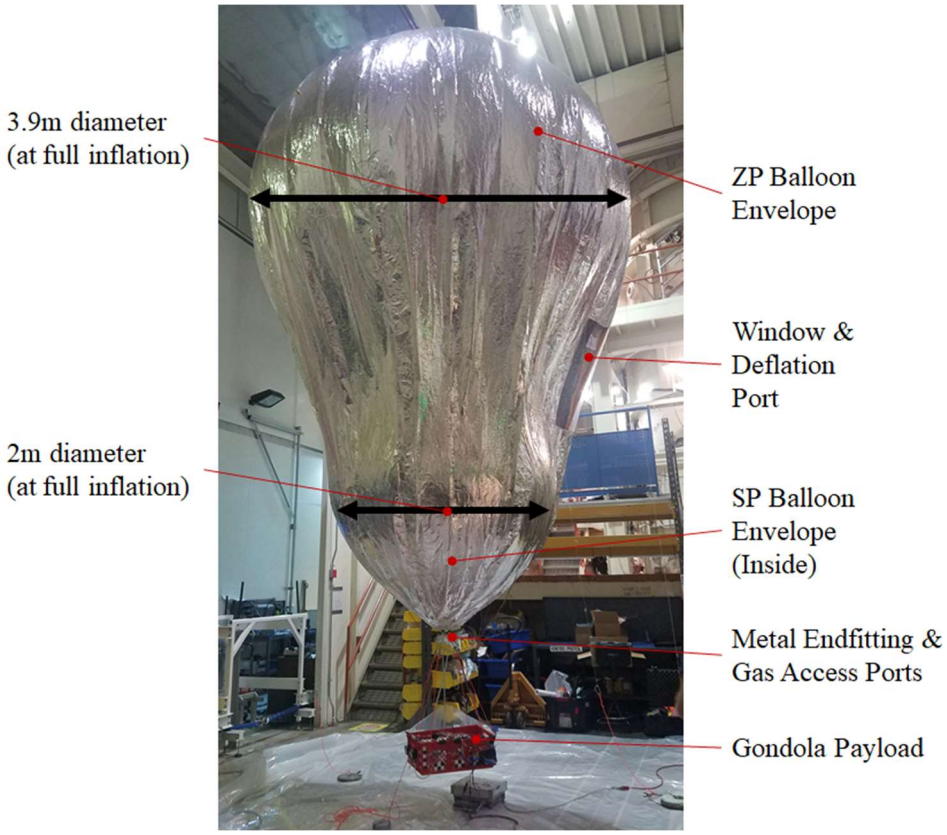

Figure 6: Subscale aerobot prototype including gondola payload, inflated indoors at JPL.

V. Prototype Test Results

Laboratory testing of the prototype (Fig. 6) was limited to small altitude excursions of just a couple of meters given the lack of access to a large indoor space at JPL. Nevertheless, the prototype was successfully flown and data collected and compared to the simulation model.

The flight test of the subscale prototype was initiated by setting the helium pressure in the SP balloon to a steady value between 1-3kPa followed by trimming the weight of the gondola so as to have a marginally negative (< 10 grams) net initial lift. The vent valve was opened to release gas from the SP balloon to the ZP balloon, leading to an increase in buoyancy and vertical rise of the aerobot. The vent valve was kept open until the ascent was complete, after which the vent valve was closed, the gate valve was opened (see Fig. 4) and the pump was turned on, moving helium back into the SP balloon. This reduced the buoyancy of the aerobot and started a descent. Due to small crosswinds in the testing facility caused by indoor air circulation, it was occasionally necessary to manually move the

balloon horizontally to prevent collisions with obstacles in the room. Several such traverses with ascents and descents at different superpressure levels were conducted. Figure 7 shows sample data from one such traverse, where an increase in altitude is seen in correlation with dropping SP pressure after the vent valve is opened, while gondola descent is noted when helium is pumped back into the SP balloon, raising its pressure. A discontinuous jump is observed when either the vent valve is opened or closed or the pump is turned on and off due to pressure line loss from tubing between the components of the pumping system as the gas transitions between static and flowing states. When comparing with results from the FLOATS simulation (see Section VI below), data "snippets" were prepared to exclude time sections when the gondola was manually moved and a correction applied for the line loss to obtain the true pressure value across the pump.

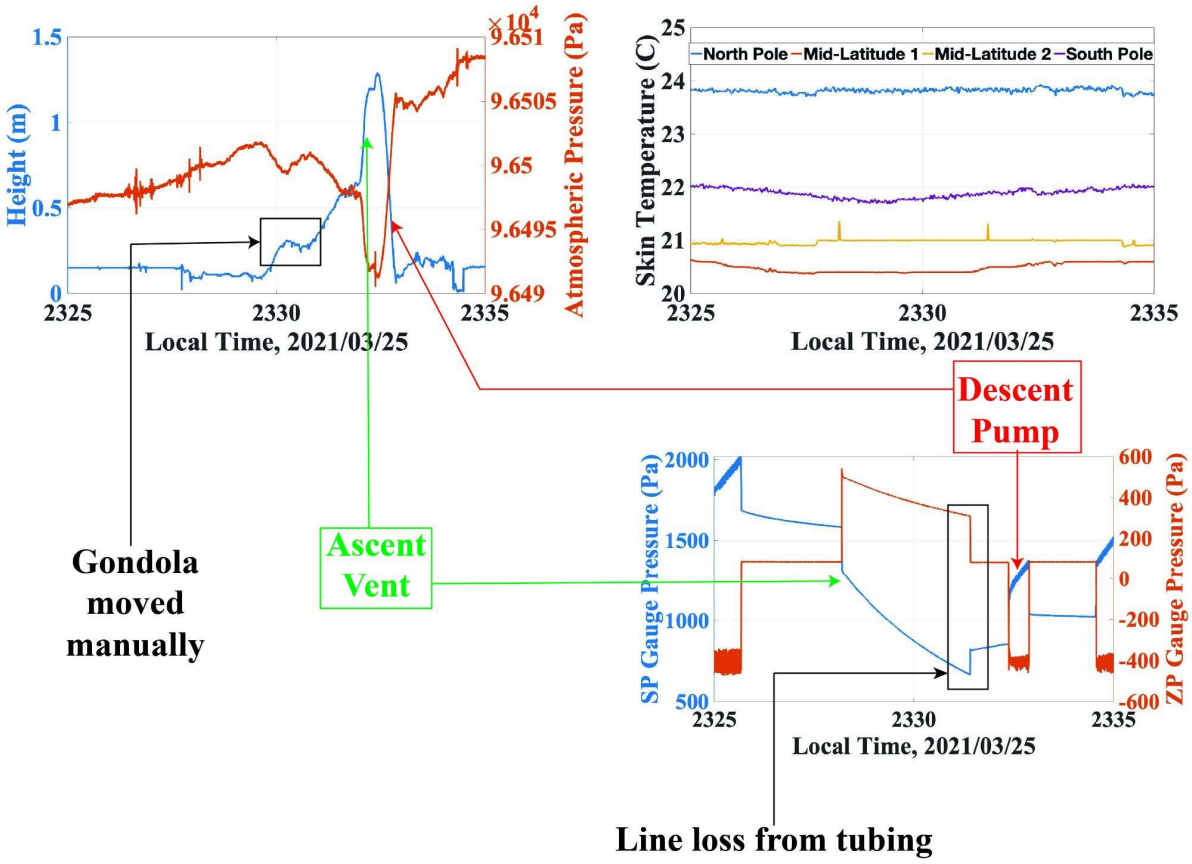

Figure 7: Sample data recorded during the subscale flight test. When helium is vented from the SP balloon to the ZP balloon, the pressure in the SP balloon drops, while the pressure in the ZP balloon remains relatively constant. The increased buoyancy results in an increase in gondola height. Conversely, when helium is pumped from the ZP balloon back to the SP balloon, SP pressure rises and the loss of buoyancy results in a drop in altitude. When the pump or vent valve are actuated, a discontinuous change in pressure is seen at the transducers. This is due to line loss from the tubing as fluid changes from a static to dynamic flow state. The skin temperature remains relatively constant during the test. During a traverse, the gondola needed to be moved manually on occasion to avoid obstacles within the testing area.

VI. Simulation Model

We have developed the FLight Operations and Aerobot Trajectory Simulator (FLOATS) simulation tool for modeling the dynamics and the thermodynamics of the aerobot. The goal of FLOATS is to provide accurate predictions of the behavior of the system for supporting missions whose conditions cannot be easily reproduced in the lab. This section provides an overview of the FLOATS simulator and validation comparisons against recent data collected from the Earth-based prototype laboratory test. Furthermore, we describe simulation results for Venus scenarios including updated design margins based on new results on the effect of vertical winds on altitude displacements.

A. Model description

The FLOATS aerobot simulator is built upon JPL's DARTS/Dshell toolkit [16] for the closed-loop simulation of autonomous space vehicles, landers, and robotics applications. The Dshell framework provides core functionality for building complex system simulations encompassing multibody dynamics coupled with environmental and actuator/sensor device models. The component Dshell models are designed for reuse and are written in C++ for speed. The system dynamics are integrated using the cvode [17] initial value solver for stiff and non-stiff ordinary differential equations. A Python interface is available for user interaction, configuration and scripting support. FLOATS allows running various simulation scenarios in different environments, using other atmospheric models and design points. In addition, FLOATS enables the selection of model configuration, environment, and design points from the command line or via configuration files. This provides a convenient way to easily switch FLOATS simulations between different scenarios on Venus and Earth and different design points.

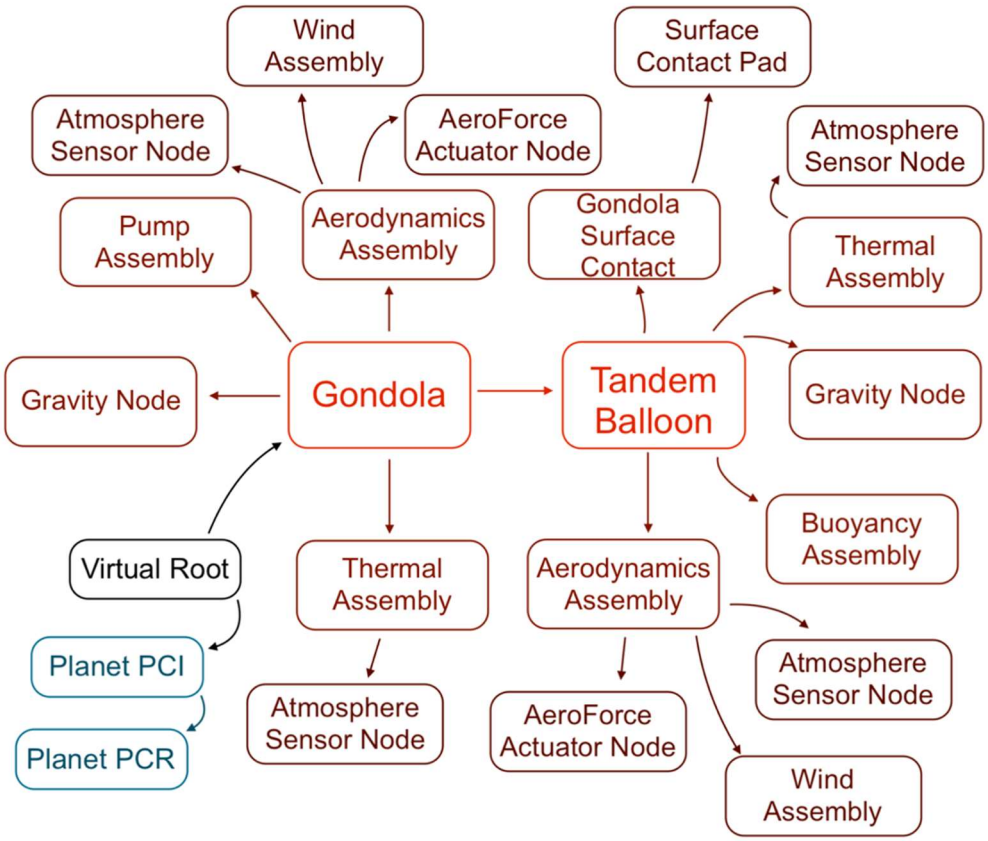

Figure 8: Schematic diagram of the tandem balloon system.

Fig 8 shows the schematic of the sub-system assemblies in FLOATS and their relationships. The planet PCR and PCI are body objects representing the planet-centered rotating and inertial frames, while the virtual root represents the inertial reference for the multibody model. The gondola body is for the scientific payload and the tandem balloon body is attached to it as a child body. FLOATS uses an N-body gravity model with spherical harmonics for Venus and Earth. The gravitational force derived from it is applied to the gondola and tandem balloon bodies. The Gondola Surface Contact assembly is a new model introduced to model the contact dynamics between the gondola and the terrain during the touch down phase for Earth scenarios.

The governing equation which governs the vertical motion of the balloon, expressed in Eq. (9), adds dynamics and virtual masses effects into the equilibrium equation originally discussed in Eq. (1).

$$(M_{total} + C_m \cdot V)\frac{d^2z}{dt^2} = (\rho_{atm} \cdot V - M_{total})g - \frac{1}{2}\rho_{atm} C_D S_{ref}\left(\frac{dz}{dt}\right)^2 \tag{9}$$

where C_m is the virtual mass coefficient, V is the aerobot volume, z is the altitude, t is time.

The current dynamic thermal model includes convection and radiation as the primary forms of heat transfer for the balloon system gases and envelopes. The heat balance equations for the gas in the ZP balloon is given by Eq. (10) as per Carlson and Horne [23].

$$m_{zp} c_g \frac{dT_{zp}}{dt} = \dot{q_{zp}} - F_{b,zp}\frac{dz}{dt} + \dot{H}_1 - \dot{H}_2 \tag{10}$$

where m_{zp} is the mass of helium gas in the zero pressure balloon, c_g is the specific heat at constant pressure for helium, T_{zp} is the temperature of helium gas in the zero pressure balloon, $F_{b,sp}$ is the gross buoyancy force generated by the helium gas in the zero pressure balloon (mass of displaced atmosphere), z is the altitude, t is the time, $\dot{H}_1$ is the enthalpy flux of the helium being added to the ZP balloon and $\dot{H}_2$ is the enthalpy flux of the gas being removed from the ZP balloon. A similar equation is used for the SP balloon.

The supported atmospheric and wind models include Venus GRAM 2005 [18] and VIRA for Venus [14], and Earth GRAM for Earth. The balloon shape model has been updated and is described in a later subsection.

The pump assembly is attached to the gondola. It computes the mass flow rate for the helium exchanged between the zero pressure and the super pressure balloons for adjusting the balloon's buoyancy. The pump and the vent flow rates are computed as in Eqs. (11) and (12), [19].

$$\dot{m}_{pump} = \rho_{zp} \cdot \dot{V}_{pump} \tag{11}$$

$$\dot{m}_{vent} = C_d \cdot \frac{\pi}{4} \cdot d^2 \cdot \sqrt{2 \cdot (P_{sp} - P_{atm}) \cdot \rho_{sp}} \tag{12}$$

where $\dot{V}_{pump}$ is the pump volume rate, d is the vent diameter, ρ is the density of the gas in the ZP and SP balloons, C_d is the discharge coefficient of the vent, and P_{SP} is the pressure in the SP balloon.

All the underlying equations used in the models are written in C++ and embedded into the tandem balloon assembly.

B. New balloon shape model

The previous shape model used in Ref. [12] consisted of two different configurations to describe the balloon's shape at high and low volume. In this shape model the SP balloon was always modeled as a sphere with constant volume and one thermal node within the ZP balloon. A node in this context is the point location for which the temperature represents all of or part of the balloon in the modeling process. When α_c, the angle between the balloon's centerline and the conical walls is positive, the ZP balloon was modeled as a sphere-cone-sphere shape with three thermal nodes, while for negative α_c it was modeled as a sphere-in-a-sphere shape.

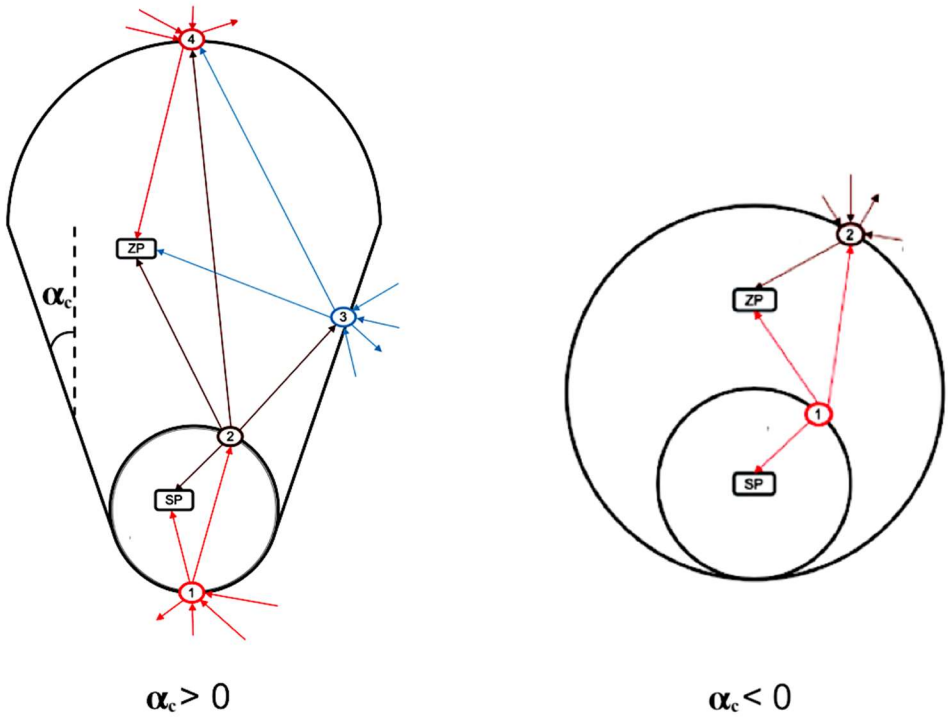

Figure 9: Previous balloon shape model, varying geometry with α_c.

This shape model suffered from several limitations. The main issue was that the sphere-cone-sphere configuration was unable to properly handle partial inflation conditions. Furthermore, the sphere-cone-sphere shape allows for a temperature gradient, while the sphere-in-a-sphere temperature was uniform for thermal equilibrium. Also, the transition between positive and negative α_c caused a discontinuity in all the shape-dependent parameters, such as aerodynamic forces, radiative view factors, film stress, and inertias. The combination of these problems made it difficult to explain the unusual behavior of the node's temperatures predicted by the model in certain scenarios.

Due to these limitations, the shape model has been updated to describe a more realistic shape subject to the constraint of constant gore length for a fully inflated ZP balloon and to model all the stages of deflation. The new model also includes necking behavior and has accurate models of secondary effects, such as heat transfer, drag force, and geometry properties. The actual shape is closer to a sphere-cone but with a narrower "peanut" midsection at low volume.

The fundamental equations for an axisymmetric fixed altitude balloon shape (see Fig. 10) from [20], are shown in Eqs. (13) to (16):

$$r_g \sigma_m \frac{d\theta}{ds} = \sigma_c \cos\theta - r_g w \sin\theta - r_g b(z - z_0) \tag{13}$$

$$r_g \frac{d\sigma_m}{ds} = \sigma_c \sin\theta - r_g w \cos\theta - \sigma_m \sin\theta \tag{14}$$

$$b = g \cdot (\rho_{atm} - \rho_{He}) \tag{15}$$

$$\frac{dr_g}{ds} = \sin\theta \qquad \frac{dz}{ds} = \cos\theta \qquad \frac{dA}{ds} = 2\pi r \qquad \frac{dV}{ds} = \pi {r_g}^2 \cos\theta \tag{16}$$

where s is the arc length along the gore, θ is the vertical tangent angle (e_3 is the vertical direction in Fig. 3), r_g is the radius along the gore, σ_c and σ_m are the circumferential and meridional stresses, b is the internal pressure slope (Eq. (15)), w is the areal density of the balloon's material, z_0 is the hydrostatic point (where the internal and external hydrostatic pressures are equal), and A and V are the balloon's area and volume.

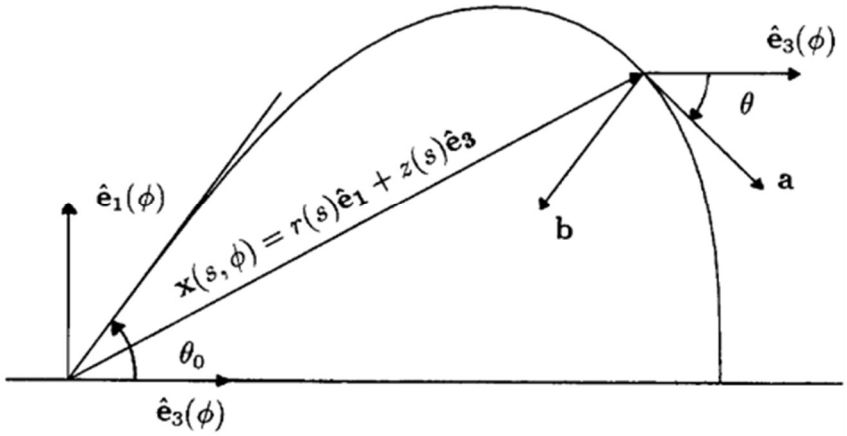

Figure 10: Axisymmetric fixed altitude balloon shape [20].

In Ref. [21], Cameron adapted Smalley's shape prediction, described in Ref. [22], modifying the boundary constraints proposed by Baginski in [20], to accommodate the SP balloon, as shown in Fig. 11.

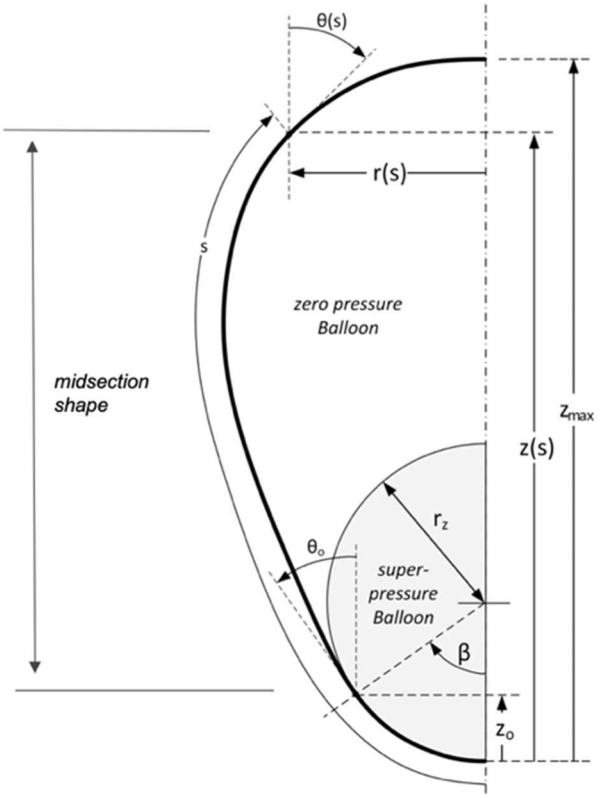

Figure 11: Axisymmetric fixed altitude balloon shape, [21].

We focused on solving the problem using the standard shooting method approach and the fundamental equations described in [21], but only for the midsection part between the bottom SP balloon and the top spherical cap of the ZP balloon. The boundary value problem has been solved using the shape equations for β and s, Eqs. (17) and (18):

$$r_g(s) = R_z \sin\frac{s}{R_z} \tag{17}$$

$$\tan\theta(s) = \frac{dr}{dz} = \frac{\cos\left(\frac{s}{R_z}\right)}{\sin\left(\frac{s}{R_z}\right)} \tag{18}$$

with $0 < \beta < \pi$ and $0 < s < L_g$. Here R_z is the outer envelope radius, and L_g is the gore length.

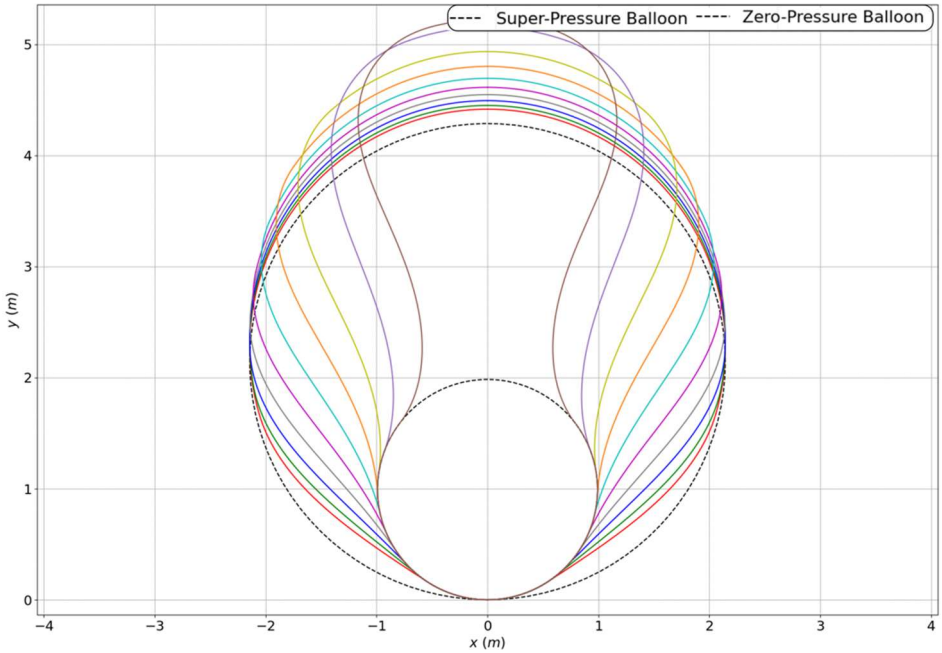

Figure 12: Updated approach: Subscale prototype shape solutions using the standard shooting method for the midsection.

Given β and the payload mass, the initial states $\theta(0)$, $\sigma_m(0)$, $r(0)$, $z(0)$, $A(0)$, and $V(0)$ are known. The balloon shape solutions for various volumes using this approach are shown in Fig. 12, where the SP and the ZP envelopes are shown as dotted lines. Figure 13 is a comparison between the balloon shape and the gore geometry.

The inputs for this updated shape model are the SP and ZP radius, payload mass, film weight per unit area, gas molar mass (helium in this case), atmospheric molar mass, gore length, gravity, and film thickness. The shape is then solved by varying the hydrostatic point and the atmospheric density. The balloon shape solutions are computed in parallel to get the results faster. Once the solutions have been found, the solver generates a lookup table that includes surface areas, view factors, characteristics lengths, geometry and inertia parameters, to be used in the thermal and buoyancy models. Multi-dimensional interpolation, based on the dilump algorithm, is used to extract parameters with respect to the atmospheric density and balloon volume. Several tests have been carried out to verify that the dilump algorithm works correctly for the new shape.

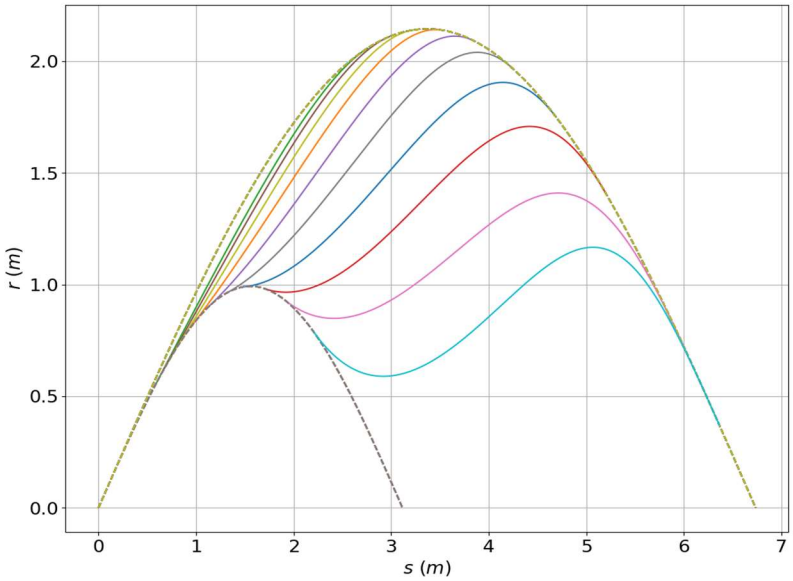

Figure 13: Radial distance versus arc length.

C. Venus test cases

Results from the Venus case have played a crucial role in deriving the balloon design margins for the range of wind conditions and pump parameters. This subsection presents the results obtained using FLOATS (Fig. 14), from the simulations carried out on Venus at different zenith angles. The time of the day plays an important role since it affects the solar and thermal fluxes used in the thermal model. For this reason, we focused on two extreme conditions: zenith values of 97 degrees (night, sun well below the horizon) and 0 degrees (noon on the equator).

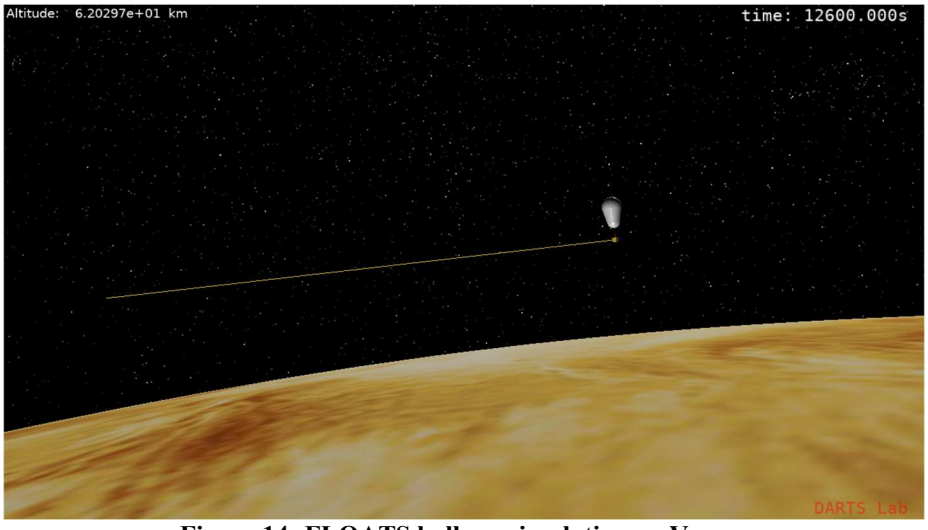

Figure 14: FLOATS balloon simulation on Venus.

Scenarios involving varying the pump rate and the vent diameter have been analyzed to understand the effect of temperature on the altitude displacement due to vertical winds.

52 km altitude case: In the first case, the balloon is placed in equilibrium at 52 km of altitude and then a constant downdraft of 3 m/s is applied for the night time zenith value of 97 degrees. As shown in Fig. 15, the aerobot experiences an initially rapid descent due to the vertical wind, but then decelerates due to the restoring force of the SP

balloon and any additional vented helium into the ZP balloon. Different sizes of vent valve orifices show the expected change in vehicle response in Fig. 15 with larger orifices arresting the descent faster. In the case without helium venting (denoted as a 0 mm vent orifice in Fig. 15) the system is still able to find a new equilibrium altitude due to the extra buoyancy generated by the SP balloon at higher atmospheric density.

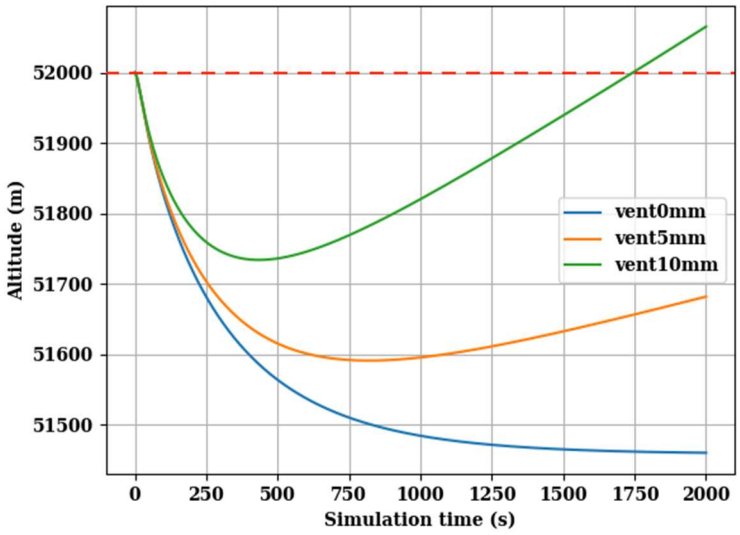

Figure 15: Vertical motion of tandem balloon with vertical downdraft of 3 m/s at night.

Fig. 16 shows the results of the same scenario at noon (zenith angle of 0 degrees). For this case, the venting compensates for the downdraft a little faster and at a slightly higher altitude due to the extra buoyancy provided by the solar-heated vented helium gas vented into the ZP balloon.

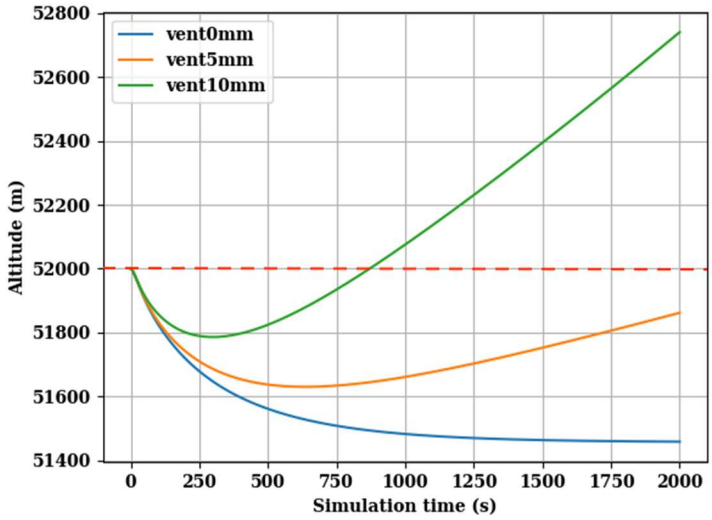

Figure 16: Vertical motion of tandem balloon with vertical downdraft of 3 m/s at noon.

62 km altitude case:

In this case, the balloon is put at equilibrium at 62 km of altitude and then subjected to a 3 m/s sustained upwards wind. Again, three different scenarios are considered. In the first one the pump is switched off and the tandem balloon stops ascending and reaches a new equilibrium because the SP balloon generates less buoyancy in the lower density at higher altitudes. In the second and third cases, the helium is pumped from the ZP to the SP balloon at a rate of 100 and 200 liters per minute, to help compensate for the wind. Fig. 17 shows the results at night time while Fig. 18 shows results from noon. The balloon shows rapid ascent due to a vertical updraft of 3 m/s, at different times of the day. The impact of the time of day is similar to that seen in the earlier 52 km case. Note that the time to compensate for the vertical downdraft at 52 km of altitude is smaller than the one to compensate for the updraft at 62 km. This is due to the fact that solar heating creates more buoyancy and tries to push the aerobot upwards. This serves to arrest the downdraft motion at low altitude but accelerates the updraft motion at high altitude making it harder to stop.

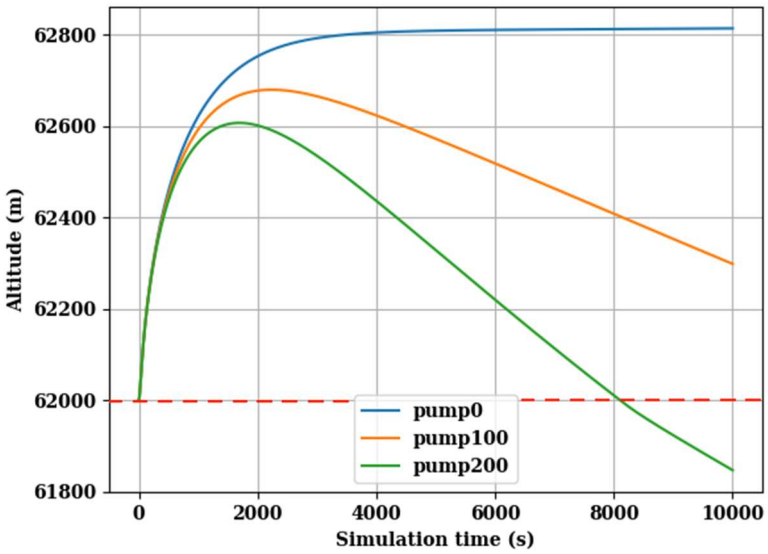

Figure 17: Vertical motion of tandem balloon with vertical updraft of 3 m/s at night.

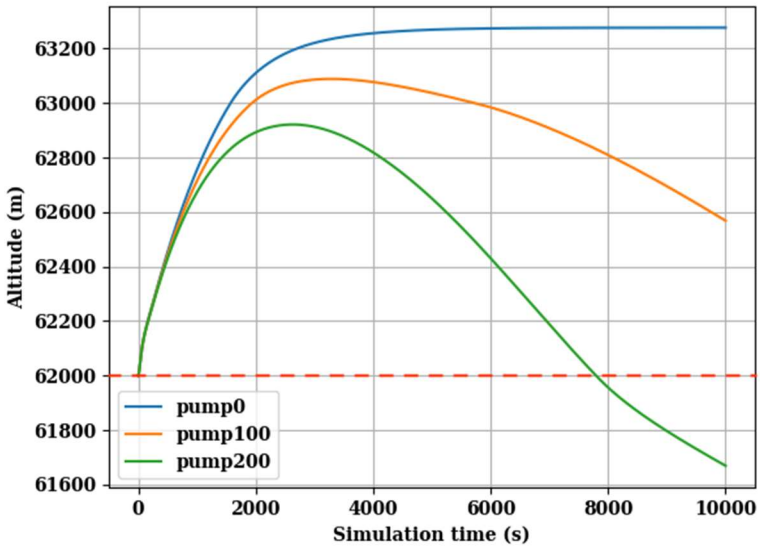

Figure 18: Vertical motion of tandem balloon with vertical updraft of 3 m/s at noon.

Continuous ascent and descent case: Additional Venus simulations have been carried out to predict the aerobot's behavior in a descent and ascent mission-like profile with a duration of roughly 23 hours and in the absence of vertical winds. The altitude versus time results are shown in Figures 19 and 20. The system starts in equilibrium at 62 km altitude. The scenario starts with pumping helium into the SP balloon for 70,000 seconds at a rate of 200 liters per minute, reaching an altitude of approximately 53.7 km. After switching the pump off, the system finds a new equilibrium at this altitude. After another 5,000 seconds, the valve is opened and the helium gas in the SP balloon flows back into the ZP balloon through a vent diameter of 10 mm. The aerobot ascent is rapid at this venting rate and reaches the original 62 km altitude in just 7,000 seconds after the start of venting.

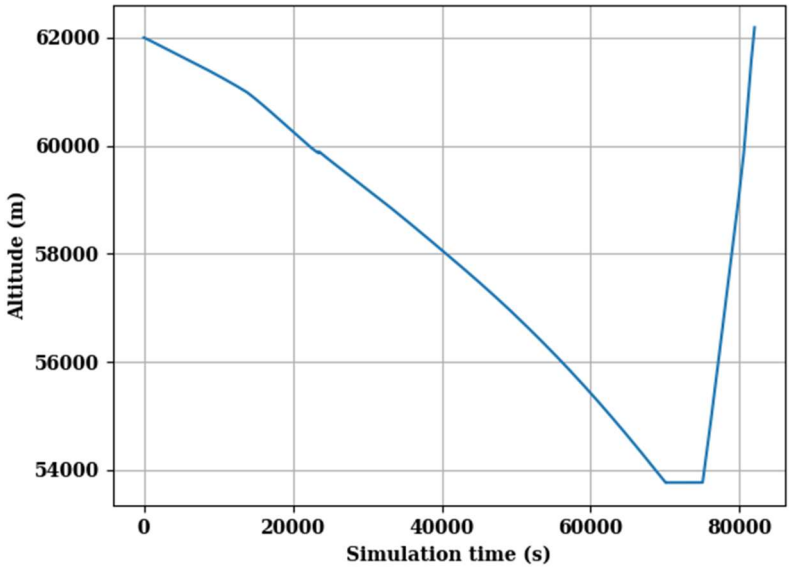

Figure 19: Vertical displacement of the tandem balloon as a function of time.

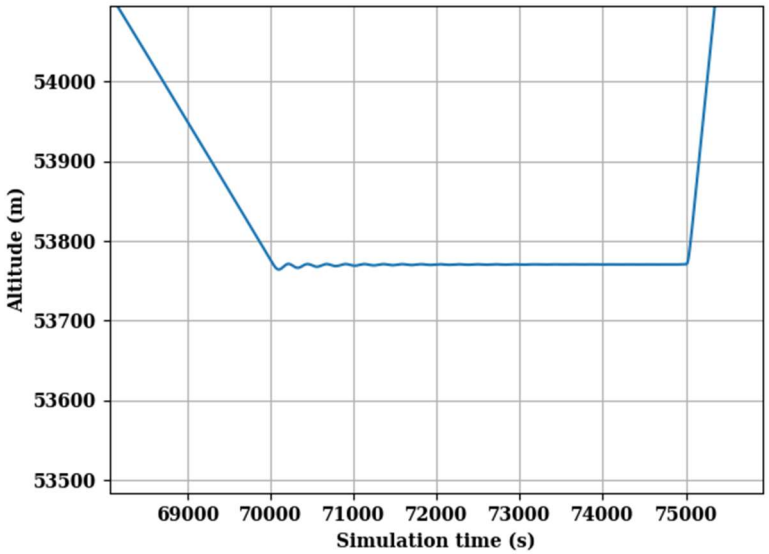

Figure 20: Close up on the equilibrium reached when the pump is switched off.

D. Earth simulation results comparison with prototype physical testing at JPL

Several simulations have been carried out and results compared with the laboratory test results described in Section V above. The recorded test data have been divided into snippets of different durations to avoid including the ground effect and human interaction with the gondola to prevent the gondola from colliding with the wall and other objects. For each snippet, the temperature at the nodes, gondola height, SP and ZP gas temperature and pressure, pumping and venting times are known. Data was recorded at different frequencies, so the first step has been to parse the data, calibrate out the head losses from the SP and ZP pressures, and convert the time of the day into simulation time.

The measured SP and ZP initial temperatures have been provided as input to the simulation, while the node's temperatures and the mass of helium inside the ZP balloon have been computed to put the balloon close to its equilibrium state. Knowing the SP pressure, SP temperature and the fixed volume of the SP reservoir, the mass of helium in the SP balloon is then computed. The venting and pumping times were also given as input to the simulation. Moreover, the atmospheric pressure and temperature coming from the recorded data has been interpolated and used as input to the simulation, based on the gondola's altitude.

Below are two examples comparing test data and FLOATS simulations, one for helium venting from the SP to the ZP balloon causing an ascent (Figs. 21) and the other helium pumping from the ZP to the SP balloon causing a descent (Fig. 23). The corresponding superpressure time histories corresponding to each case are shown in Fig. 22 and Fig. 24 respectively. Good agreement is seen in each case.

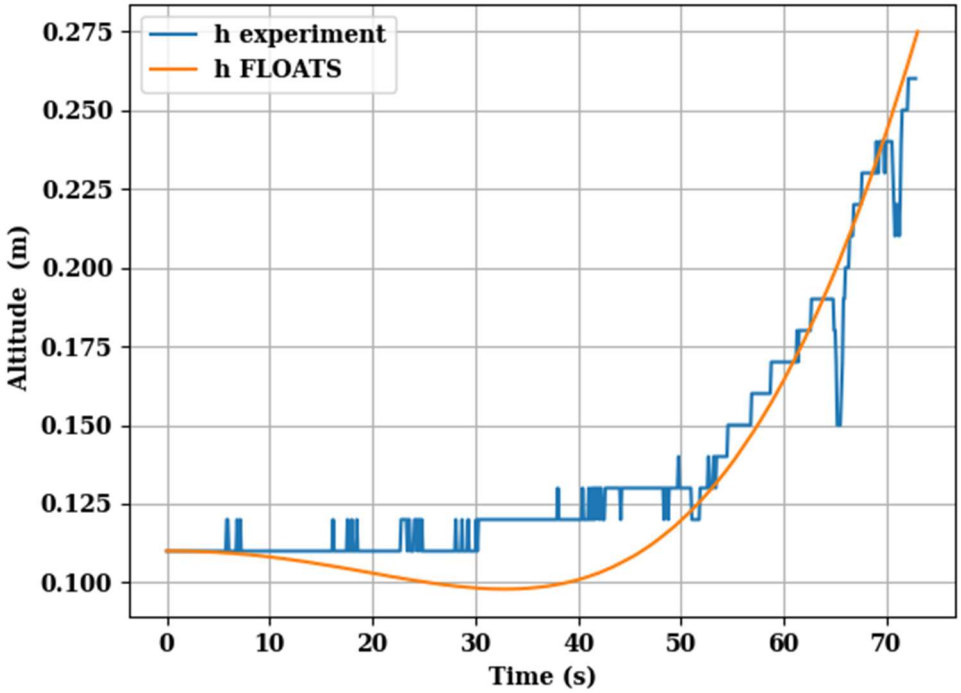

Figure 21: Venting through a 2.5 mm orifice: gondola altitude versus time.

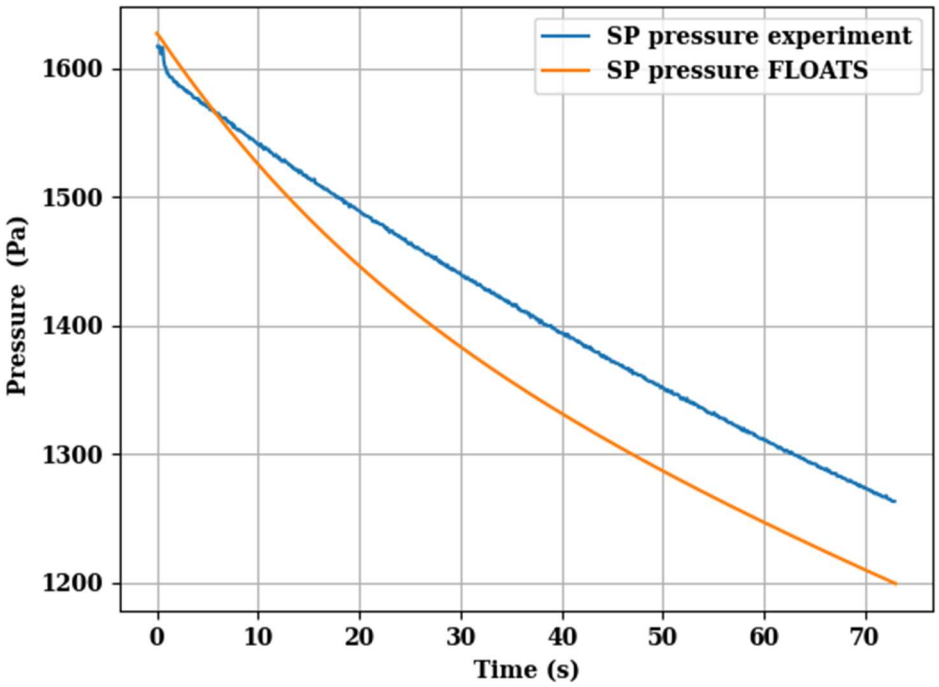

Figure 22: Venting case: SP balloon superpressure versus time.

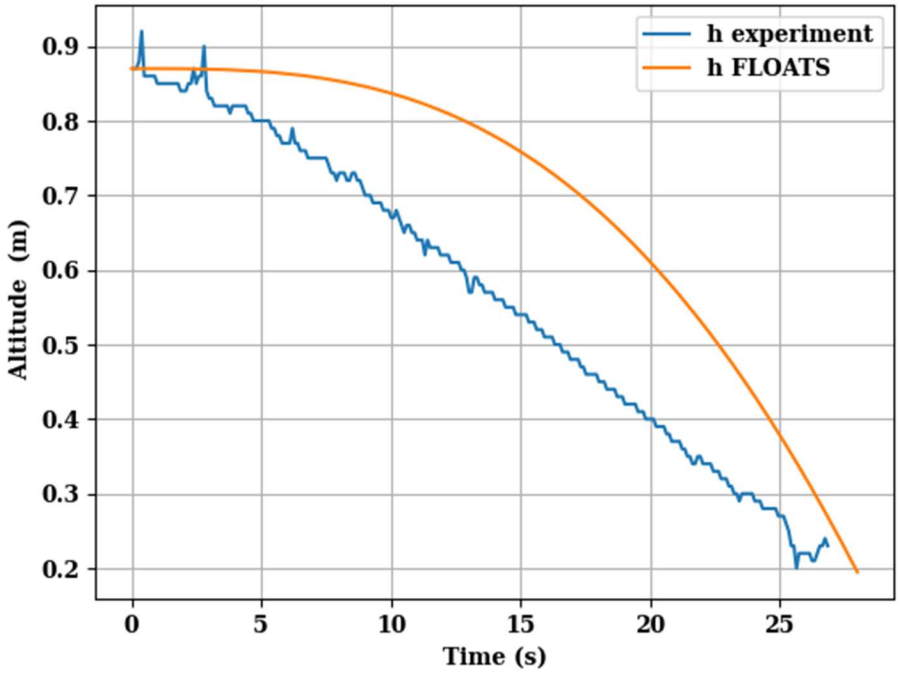

Figure 23: Pumping at 11 m/s: gondola altitude versus time.

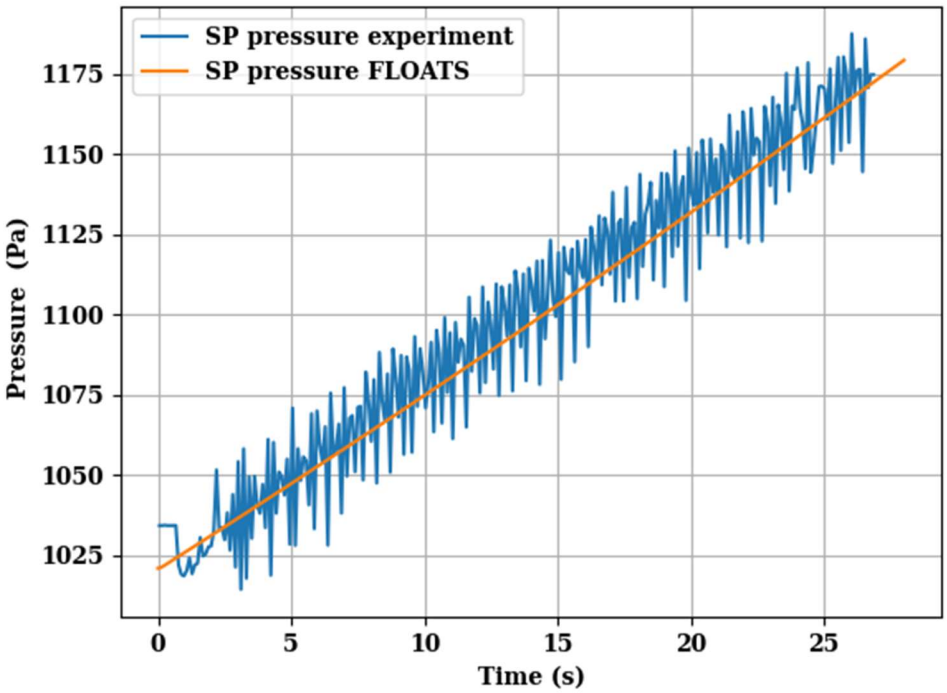

Figure 24: Pumping at 11 liters/s: SP balloon superpressure versus time. The jagged sawtooth-like structure in the measured superpressure are caused by the pumping action of the positive displacement pump used in the experiment.

VII. Conclusion

This paper has described the design, simulation, fabrication and testing of the first subscale prototype Venus aerobot based on the balloon-in-a-balloon concept. This moderate fidelity prototype achieved the goals of the technology development activity by revealing and solving manufacturing challenges, successfully floating in the laboratory environment and providing initial data with which to start the validation process for the FLOATS simulation tool. These accomplishments will lead into the next development phase that will produce high fidelity subscale prototypes to be used in Earth atmosphere flight testing across the 0 to 11 km altitude range that matches the atmospheric density to be encountered across the expected 52 to 62 km altitude range at Venus. These flight tests will not only provide data to continue validation of the FLOATS simulation tool but will also help validate the fundamental balloon thermodynamics theory and design margin strategy described in this paper and its precursor [12].

Acknowledgments

The research described in this paper was funded by the Jet Propulsion Laboratory, California Institute of Technology, under a contract with the National Aeronautics and Space Administration. The authors would like to thank the occupants of Building 248 at JPL, and especially the CITADEL team, for the use of their space for balloon testing.

References

[1] R. Z. Sagdeev, V. M. Linkin, J. E. Blamont and R. A. Preston, “The VEGA Venus Balloon Experiment”, Science, Vol. 231, pp. 1408-1408, March 1986.
[2] J. A. Jones, “Reversible Fluid Balloon Altitude Control Concepts”, AIAA Paper 1995-1621.
[3] R. E. Schied, M. K. Heun, J. M. Cameron and J. A. Jones, “Thermodynamics, Phase Change, and Mass Transfer in Oscillatory Balloon Systems (Aerobots)”, AIAA Paper 1996-1870.
[4] K. T. Nock, K. M. Aaron, J. A. Jones, “D. P. McGee, G. E. Powell, A. H. Yavrouisn and J. J. Wu, “Balloon Altitude Control Experiment (ALCIE) Project”, AIAA Paper 1995-1632.
[5] A. Bachelder, K. Nock, M Heun, J. Balaram, J. Hall, J. Jones, V. Kerzhanovich, D. McGee, E. Stofan, J. Wu and A. Yavrouian, “Venus Geoscience Aerobot Study (VEGAS), AIAA Paper 1999-3856.

[6] J. L. Hall, D. Fairbrother, T. Frederickson, V. V. Kerzhanovich, M. Said, C. Sandy, C. Willey and A. H. Yavrouian. "Prototype design and testing of a Venus long duration, high altitude balloon", Advances in Space Research, Vol. 42, pp 1648-1655, 2008.
[7] J. L. Hall, V. V. Kerzhanovich, A. H. Yavrouian, G. A. Plett, M. Said, D. Fairbrother, C. Sandy, T. Frederickson, G. Sharpe, and S. Day. "Second generation prototype design and testing for a high altitude Venus balloon", Advances in Space Research, Vol. 44, pp. 93-105, 2008.
[8] Venus Aerial Platforms Study Team, "Aerial Platforms for the Scientific Exploration of Venus", JPL D-102569, October, 2018.
[9] https://loon.com/
[10] https://worldview.space/
[11] Voss, Paul B., "Advances in Controlled Meteorological (CMET) Balloon Systems", AIAA Paper 2009-2810, May 2009.
[12] Jeffery L. Hall, Jonathan M. Cameron, Michael T. Pauken, Jacob S. Izraelevitz, Mitchell W. Dominguez, Kristopher T. Wehage, "Altitude-Controlled Light Gas Balloons for Venus and Titan Exploration", AIAA Paper 2019-3194, presented at the AIAA Aviation Forum, Dallas, TX, June 17 to June 21, 2019.
[13] M. S. Gilmore, P. M. Beauchamp, R. Lynch and M. J. Amato, "Venus Flagship Mission Decadal Study Final Report", A Planetary Mission Concept Study Report Presented to the Planetary and Astrobiology Decadal Survey, 08 August 2020.
[14] Kliore, A, V. I Moroz, G. M Keating, and COSPAR. The Venus International Reference Atmosphere. Advances in Space Research, Vol. 5, No. 11. Oxford: Published for the Committee on Space Research by Pergamon, 1986.
[15] T. D. Robinson and D. Crisp, Linearized flux evolution (life): A technique for rapidly adapting fluxes from full-physics radiative transfer models, Journal of Quantitative Spectroscopy and Radiative Transfer 211 (2018) pp. 78–95.
[16] https://dartslab.jpl.nasa.gov
[17] Serban, R. and Hindmarsh, A.C., "CVODES: the sensitivity-enabled ODE solver in SUNDIALS", In ASME 2005 international design engineering technical conferences and computers and information in engineering conference. pp. 257-269. American Society of Mechanical Engineers. January 2005.
[18] https://software.nasa.gov/software/MFS-32314-1
[19] https://en.wikipedia.org/wiki/Orifice_plate
[20] Baginski, Frank, Tami Williams, and William Collier. "A parallel shooting method for determining the natural shape of a large scientific balloon." *SIAM Journal on Applied Mathematics* 58.3 (1998): 961-974.
[21] Harsh P. Patel and Jonathan Cameron M. *Jet Propulsion Laboratory, California Institute of Technology, Pasadena, CA, 91101, USA.* "Natural Shapes of Tandem Balloons"
[22] Smalley, Justin H. "Determination of the Shape of a Free Balloon." *AFCRL-64-734* (1963).
[23] Leland A. Carlson and Walter J. Horn, "New Thermal and Trajectory Model for High-Altitude Balloons", J. Aircraft, Vol. 20, No. 6, p 500-507, 1983.